J Mater Sci (2024) 59:22344–22362

Polymers & biopolymers

Influence of moulding processing on poly (lactic acid) (PLA) semi-crystalline properties

Giovanna Molinari[1,2,3], Laura Aliotta[1,3,*], Paola Parlanti[2], Mauro Gemmi[2], and Andrea Lazzeri[1,3]

[1] *Department of Civil and Industrial Engineering, University of Pisa, 56122 Pisa, Italy*
[2] *Electron Crystallography, Center for Materials Interfaces, Istituto Italiano di Tecnologia, 56025 Pontedera, Italy*
[3] *National Interuniversity Consortium of Materials Science and Technology (INSTM), 50121 Florence, Italy*

Received: 16 September 2024
Accepted: 21 November 2024
Published online: 4 December 2024

ABSTRACT

Poly (lactic acid) (PLA) is a bio-based and compostable polyester, widely employed in a variety of daily used products, being easily processed via the traditional manufacturing techniques, i.e., injection moulding (IM), compression moulding (CM), blow moulding (BM), etc. This study will be specifically focused on the impact of both IM and CM processing techniques on PLA characteristics, aiming to optimize these manufacturing procedures and ultimately improving its end-products features. By means of thermal, mechanical and microscopy analysis, the role of the different moulding techniques in influencing the PLA semi-crystalline development will be extensively investigated, also by correlating the related morphology with its macroscopical behavior. It will be observed that the polymer flow orientation during IM promotes the semi-crystalline development, as confirmed by Avrami analysis, XRD measurements, and TEM imaging. Moulded sample thickness, manufacturing pressure, and PLA granular consolidation that differ for the two moulding methodologies appear to be directly accountable for the detected faster crystallization kinetics during IM when compared to the CM one. Finally, by combining thermal information (Gibbs–Thomson equation), XRD data (Scherrer equation) and TEM imaging, the size of the crystalline lamellae during PLA crystallization will be sampled, also detecting the phenomenon of "lamellar thickening" as the crystalline content increases in both the injection and compression moulded samples.

Introduction

Driven by the strong demand of the current worldwide scenario, bioplastics market accounts for steadily expanding, with a predicted annual growth rate between 10 and 15% by 2025 [1]. Among them, poly (lactic acid) (PLA), a totally bio-based and biodegradable polyester capable of competing with the traditional plastics in terms of performance, is one of the most appealing.

PLA can be used for several applications (e.g., packaging materials [2], disposable cutlery [3], medical

Handling Editor: Chris Cornelius.

Address correspondence to E-mail: laura.aliotta@unipi.it

https://doi.org/10.1007/s10853-024-10497-8

implants [4]), becoming a promising alternative to petrol-derived plastics for addressing the growing ecological issue of plastic waste, with a particular emphasis on packaging. Indeed, given that plastic packaging has a short lifespan of fewer than six months before being discarded, it represents one of the major contributors to plastic pollution [5]. For instance, in 2015 [6], 448 million tons of plastics were worldwide generated and about 161 million tons of that utilized for packaging materials [7].

Packaging materials are frequently required to guarantee shelf life and upkeep high-quality products during storage, transportation, and sale. Thus, packaging materials must possess a number of essential qualities, including the finest potential thermal stability and mechanical strength [8], the capacity to inhibit the growth of microorganisms [9], and the ability to prevent the exposure to water [10], vapors, and gases [11].

Polymers quality is defined by their inherent functionality and long-term stability. These aspects are, in turn, directly bound to the material structure formed by melt solidification or cooling [12] and so linked to the crystalline phase that develops during the processing stages.

Crystalline phase plays a key-role, affecting the properties of the final product (i.e., mechanical [13], biodegradation capability [14] and other physical properties [15]). For instance, by increasing the polymer crystallinity, flexural strength and elastic modulus show a net increment; while, the strain at break decreases compared to the corresponding values for an amorphous material [16–19]. Moreover, the occurrence of a crystalline development can lead to a brittle fracture for the material failure, with the absence of any yielding phenomena commonly associated with the more ductile amorphous samples [20]. Regarding the barrier properties, helium shows a high sensitivity to the density variation of the polymeric phases, with a decrease in its associated permeability coefficient with the increase in the crystalline content [21]. Oxygen, instead, displays a slight decrement in its permeability coefficient with a rise of the diffusion one when the crystalline content increases [22, 23]. The crystalline content also affects the polymers thermal features because the formation ordered structure generally enhance the thermal resistance and load bearing capacity of the material [24].

In this study, the crystallization in both injection (IM) and compression moulded (CM) PLA samples together with the two processing methodologies impact on their physical/chemical properties will be analyzed. Preliminary isothermal crystallization tests will be carried out to determine distinct moulding times from which diverse crystallization contents will be attained for both the injection and compression moulded samples. Then, an access to relevant information with a view to a simultaneous survey on both the macro- and microscopic behavior of the isothermally crystallized PLA samples (110 °C) will be proposed, by means of some theoretical models (Avrami, Scherrer and Gibbs–Thomson equations) along with the interpretation of FTIR spectra, X-ray Diffraction (XRD) measurements, mechanical analysis, and transmission electron microscopy (TEM) imaging investigations. This to find a "connecting bridge" between PLA characteristics on two different scales with the final goal of providing a detailed understanding on how the two most widely used processing methodologies for PLA can impact the features of its related end-products, with a particular regard to the semi-crystalline ones.

Materials and methods

Materials

Commercial PLA Ingeo 3100HP (here named PLA) derived from natural resources was purchased from NatureWorks LLC. According to the producer datasheet, this PLA contains about 0.3% of D-lactic acid units [MFR: 24 g/10 min (210 °C, 2.16 kg); nominal average molar mass: 120,000 g/mol; density: 1.24 g/cm^3].

Injection moulding

Before injection moulding, PLA granules were dried in a DP604–615 PIOVAN dryer (Venezia, Italy) at 60 °C for 24 h. Injection moulding was carried out on a Megatech H10/18 injection moulding machine (TECNICA DUEBI S.r.l. Fabriano, Italy), to obtain ISO 527-1A dog-bone specimens (width: 10 mm, thickness: 4 mm, length: 80 mm). Amorphous and semi-crystalline PLA specimens were prepared by varying the mould holding time (t_{mould}), according to the performed isothermal crystallization measurements (see below). The temperature profile adopted was: 185/190/185/180 °C, from the hopper to the die, with an injection pressure of 90 or 190 bar for semi-crystalline or amorphous

samples, respectively. The mould was kept at 110 °C (semi-crystalline samples) or 60 °C (amorphous samples) (Fig. 1). After processing, PLA specimens were quickly cooled to room temperature (T_{room}) in less than 1 min by means of liquid nitrogen. Then, the specimens were placed in a dry keeper (SANPLATEC Corp. (Osaka, Japan)) at T_{room} and 50% humidity for 3 days before further characterizations.

Compression moulding

Before compression moulding, PLA granules were dried in a DP604-615 PIOVAN dryer (Venezia, Italy) at 60 °C for 24 h. The dried granules were compression moulded in a NOSELAB ATS (Milano, Italy) compression moulding machine, to obtain films with an average thickness of 150 µm. The parameters adopted during the moulding were: hot plates temperature of 190 °C, pressure of 390 bar and residence time of 3 min (Fig. 1). After compression moulding, the semi-crystalline specimens were rapidly transferred into a vacuum oven and annealed at 110 °C for the same t_{mould} adopted for the injection moulded samples. After annealing, PLA specimens were quickly cooled to T_{room} in less than 1 min by means of liquid nitrogen and placed in the dry keeper (SANPLATEC Corp., Osaka, Japan) for 3 days, as described above.

Tensile tests

Tensile tests for the injection moulded samples were carried out at T_{room} on ISO 527-1A dog-bone specimens using an MTS Criterion model 43 (MTS Systems Corporation, Eden Prairie, MN, USA) universal tensile testing machine, at a crosshead speed of 10 mm/min, equipped with a 10 kN load cell and interfaced with a computer running MTS Elite Software. At least 5 specimens were tested for each selected mould holding time.

For the compression moulded specimens, ISO 527-2 type A dumbbell specimens were cut with a Manual ELASTOCON Cutting Press EP 08 (Brahmult, Sweden) to carry out tensile tests at T_{room} with an INSTRON 5500R Universal Testing Machine (Canton, MA, USA) equipped with a 100 N load cell at 10 mm/min and interfaced with MERLIN software (INSTRON version 4.42 S/N-014733H). At least 5 specimens were tested for each selected mould holding time. The evaluation of the elastic moduli for the compression moulded specimen was carried out on a Gabo Eplexor® (Ahlden, Germany) with a 100 N load cell. Five specimens were tested for each sample. During the test, the constant temperature and frequency were of 25 °C and 1 Hz, respectively.

FTIR characterization

FTIR spectra were recorded for both the injection and compression moulded samples, at T_{room} in the 1780–1720 cm^{-1} range, by means of a Nicolet 380 FTIR spectrometer (Thermo Fisher Scientific, Madison, WI, USA) equipped with a smart iTX ATR accessory.

XRD analysis

XRD data were acquired in transmission/Debye–Scherrer geometry using a STOE Stadi P diffractometer equipped with Cu X-ray tube monochromated on

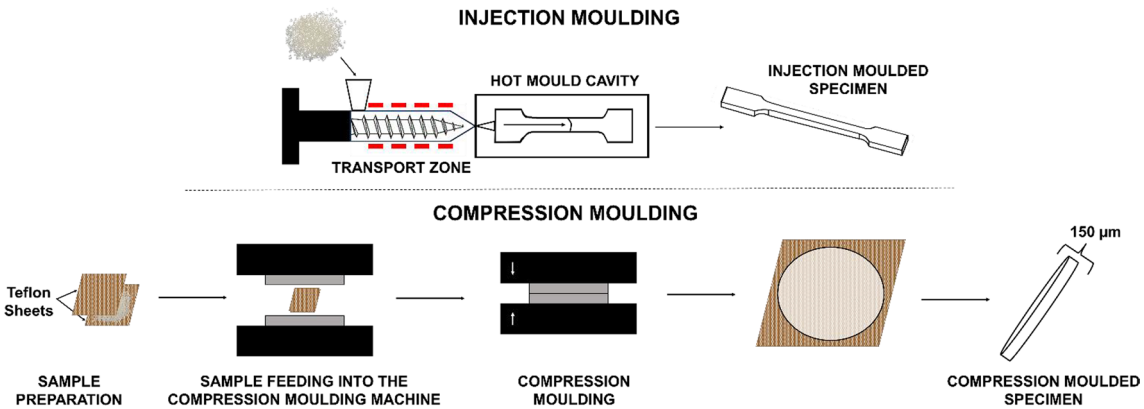

Figure 1 Schematization of injection and compression moulding processing.

the Cu-Kα_1 radiation (λ = 1.5406 Å) by a Ge (1 1 1) Johansson monochromator from STOE & Cie and a MYTHEN2 1 K detector from Dectris. The line focused Cu X-ray tube was operated at 40 kV and 40 mA. Data were acquired in the 2θ range 2–60° (maximum resolution around 1.5 Å) with an interval of 0.03° between consecutive points for both the injection and compression moulded specimens. A scan without samples was performed and appropriately scaled for each scan, to subtract the air scattering contribution. The X-ray crystalline fractions (X_C^{XRD}) were calculated as the ratio of the areas of the crystalline peaks to the total area of the background corrected diffraction profile. The lattice constants were calculated from the positions of the most XRD intense peaks. The diffraction from the crystallographic planes corresponding to the most intense XRD peaks was also analyzed with the aim of determine the lamellar thickness, according to Scherrer formula:

$$L_{hkl} = \frac{K\lambda}{B\cos(\theta)} \quad (1)$$

where L_{hkl} is the crystalline lamella thickness, K is the dimensional shape factor, also known as the Scherrer constant, λ is the radiation wavelength, B is the full width at half maximum (FWHM) value of different peaks and θ is the Bragg angle.

Thermal characterization

Differential scanning calorimetry (DSC) analysis was performed on a DSC Q200 TA-Instrument (New Castle, UK) equipped with an RSC (radiative sky cooler) cooling system. For all measurements, nitrogen was adopted as purge gas (set at 50 mL/min). The instrument was calibrated with indium, used as standard for temperature and enthalpy calibrations. The materials used for DSC were cut from the injection moulded specimens. About 10–15 mg of PLA were sealed inside aluminum hermetic pans and each sample was tested only once.

Preliminary isothermal kinetical measurements

The analysis was carried out by submitting the PLA granules to a similar thermal history of the different types of processing that will be carried out during the two sample preparation modes (Fig. 1). In this way, the recorded exothermic curves of heat flow as a function of time allow to estimate the crystallization kinetics for both the moulding procedures. For the injection moulding, the sample was firstly kept at 25 °C for 1 min, heated to 190 °C at 20 °C/min and held at 190 °C for 1 min. Then, it was cooled at 100 °C/min to 110 °C and held for 30 min. Finally, the sample was cooled down to the initial temperature of 25 °C. Conversely, for the compression moulding, the sample was firstly kept at 25 °C for 1 min, heated to 190 °C at 20 °C/min and held at 190 °C for 3 min. Then, it was cooled at 5 °C/min to 110 °C and held for 30 min. Finally, the sample was cooled down to 25 °C.

Crystallization behavior evaluation

The evaluation of the crystallization behavior of each sample was carried out by firstly keeping the specimens at 25 °C for 2 min, then heated at 20 °C/min to 190 °C and held at 190 °C for 2 min. The melting temperature (T_m) and the cold crystallization temperature (T_{cc}) were determined by considering the maximum of the melting peaks and the minimum of the cold crystallization peak, respectively. The melting and cold crystallization enthalpies were determined from the corresponding peak areas of the thermograms. The crystallinity percentage of PLA was calculated according to the following equations:

$$\chi_c = \frac{(\Delta H_m - \Delta H_c)}{\Delta H_m^0 \cdot X_{PLA}} \quad (2)$$

where ΔH_m and ΔH_{cc} are the melting enthalpy and the enthalpy of cold crystallization of PLA, respectively, X_{PLA} is the PLA weight fraction in the formulation and ΔH^0_m is the melting enthalpy (equal to 93 J/g [25]) of the 100% crystalline PLA.

Sectioning

Small PLA blocks (approx. 5 mm sides) were obtained from the IM_PLA samples by using a jigsaw and further trimmed down to approx. 1 mm each side. By using a UC7 ultramicrotome (Leica Microsystem, Vienna, Austria) equipped with a 45° diamond knife (DiATOME, Nidau, Switzerland), samples were sectioned either perpendicularly or parallelly to the direction of the polymeric flow during the injection moulding (respectively, “inner face” and “front face” in Fig. 2) in 90 nm thin slices for TEM analysis and

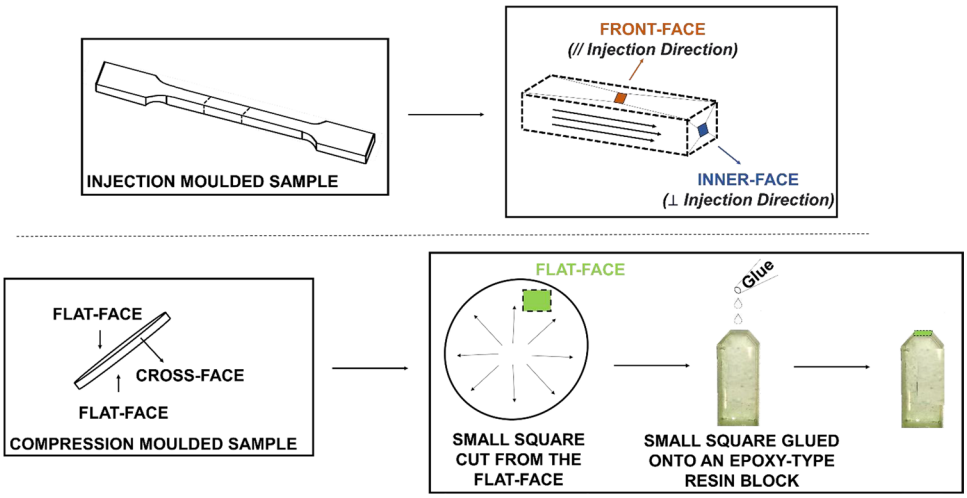

Figure 2 Schematization of the injection (IM) and compression (CM) sectioning procedures.

then collected on TEM Cu grids [EMS (Hatfield, PA, USA)].

Small squares of approximately 3 mm side of CM_PLA samples were cut and glued onto blocks of epoxy resin. After reducing the CM film resin block face to approximately 1 mm each side, thin slices for TEM were cut in the parallel direction to the polymeric flow and then collected on the TEM Cu grids (Fig. 2).

Transmission electron microscopy imaging

According to the previous study on the optimum procedure for TEM imaging of bio-polymeric samples [26], PLA thin sections placed on 300 mesh Cu grids were coated with a few nanometers of carbon to reduce charging artifacts and improve TEM imaging, by means of an EM ACE600 (Leica Microsystems, Vienna, Austria). Then, the carbon-coated sections were imaged by using a Zeiss Libra 120 Plus transmission electron microscope, operating at 120 kV equipped with an in-column omega filter (Carl Zeiss, Oberkochen, Germany), and by a bottom mounted 16-bit CCD camera 2 k × 2 k (TRS).

Results

Isothermal crystallization kinetics analysis

The IM and CM isothermal kinetical behaviors of PLA are shown in Fig. 3a, evaluated according to the procedure described in the "*Preliminary Isothermal Kinetical Measurements*" section. Their analysis is here proposed by using the Avrami approach [27]. According to the Avrami theory, the relative degree of crystallinity develops with crystallization time that is [28]:

$$1 - X(t)_t = 1 - \exp\left(-kt^n\right) \tag{3}$$

where n is the Avrami index, and k is the crystallization rate constant involving both nucleation and growth rate parameters. $X(t)_t$ is the partial enthalpy obtained by integrating isotherms up to time t and ΔH^0 is the total enthalpy of crystallization that corresponds to the total area of the isotherm:

$$X(t)_t = \frac{\Delta H(t)}{\Delta H^0} \tag{4}$$

By applying logarithmic properties to both sides of Eq. 3, the equation can be linearized as:

$$\log\left(-\ln\left(1 - X(t)_t\right)\right) = \log k + n \log t \tag{5}$$

The Avrami model also defines the half-time of crystallization ($t_{0.5}$) that is the time when $X(t)_t$ is equal to 0.5, and it is calculated as follows:

$$t_{0.5} = \left(\frac{\ln(2)}{k}\right)^{\frac{1}{n}} \tag{6}$$

The calculation of n and k (slope and intercept of their linear fit) was performed by fitting the data in a double-logarithmic plot (Fig. 3c) with a reached correlation coefficient of 0.99 for IM_PLA and of 0.96 for CM_PLA sample in the conversion range of 3–10%, to minimize the relative error on fitting [29]. The

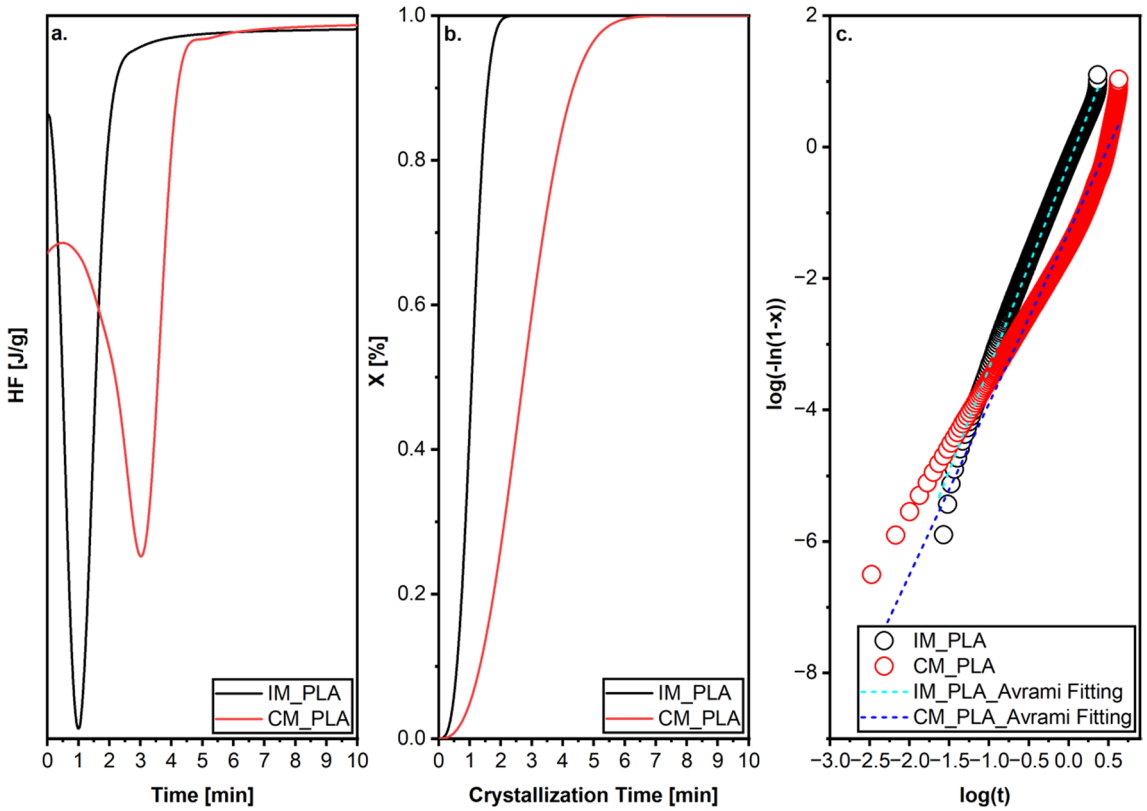

Figure 3 **a** Isothermal curves, **b** crystallized fraction percentage and **c** Avrami plots of the experimental data obtained from the isothermal crystallization for both injection and compression moulding.

Table 1 Avrami kinetic parameter and crystallization half-time for the isothermal crystallization of the IM_PLA and CM_PLA scans

Sample	n	k	$t_{0.5}$ (min)
IM_PLA	3.1	$5.68 \cdot 10^{-1}$	1.1
CM_PLA	2.6	$5.08 \cdot 10^{-2}$	2.6

estimated n values are very similar to those reported in literature for pure PLA isothermally crystallized at 110 °C [28].

In case of polymers, only $n = 2$ and $n = 3$ values are commonly obtained as they would represent axialites (two dimensional lamellar aggregates) and spherulites (superstructural three-dimensional aggregates of radial lamellae), respectively. The Avrami exponent values for the two types of industrial moulding are reported in Table 1 ($n = 3.1$ for IM_PLA specimens and $n = 2.6$ for CM_PLA ones). This difference can be ascribable to the moulded sample thickness (4 mm for IM_PLA and 150 µm for CM_PLA). Indeed, due to the poor thermal conductivity of polymers, thicker IM_PLA samples cool more slowly. Generally, the slower the cooling process, the greater the sample crystallinity, because the polymer chains have a longer time to arrange themselves into ordered arrangements [30] and thus to crystallize. So, the greater moulded sample thickness facilitates the crystalline development, here represented by a higher Avrami exponent value (higher crystallites dimensionality) for injection moulding.

The nucleation rate appears kinetically favored in the case of IM samples, as evidenced by the one order of magnitude higher k-values, evidence also confirmed by the $t_{0.5}$ values. Indeed, for the CM_PLA, more than twice the time is required to reach half the total attainable crystallization rate, as also detectable (red curve) in Fig. 3b.

Thermal analysis of IM_PLA and CM_PLA samples

The crystalline content at different mould holding time for the two different processing methodologies are

reported in Fig. 4. Both IM_PLA and CM_PLA samples display a progressive increase in the crystalline content, reaching final values of 30 and 33%, respectively. These values agree with the crystalline content estimated by means of the XRD analysis (Fig. 8c, d).

For the injection moulded specimens, the crystallization rate is faster, confirming what is observed by means of the Avrami approach: Higher crystalline contents are achieved more quickly. However, for the compression moulded specimens, the reached crystallinity (20 min) is slightly higher than that of injection moulded samples. Various aspects strictly connected with the type of moulding come into play. One of these is the improvement of granular consolidation during compression moulding. According to Xie et al. [31], the polymer melt has a memory of its original granular shape in the microstructure. It is known that to achieve a final well-formed crystalline phase, two conditions must be complied during the melting stage of the processing [32]. Firstly, the adjacent faces of the polymer granules must be in close contact and, secondly, the polymer chains must interfere across these boundaries. The first process is largely controlled by the pressure applied, while the second one by chain diffusion/reptation of the polymeric chains within the melt. Therefore, a higher pressure and a longer mould holding time (which results into longer time to polymer reptation) before annealing have facilitated the crystalline development in CM_PLA samples. Also, the better granular consolidation for compression moulded specimens results in polymer chains having fewer "spatial obstacles" in their movements than in the case of injection moulding process, favoring simpler ordered arrangements, and thus promoting the eventual crystalline development. Finally, as will be pointed out in the section dedicated to the TEM characterization from the results of the isothermal analysis, injection moulding shows an instantaneous nucleation while, compression moulding, a continuous nucleation stage, which will lead to the presence of a greater number of nuclei in the compression moulded samples (see Fig. 10). As a result, over extended annealing times, the growth of a greater number of spherulites (CM_PLA samples) will contribute more significantly to the overall crystalline content than when presence of fewer formed spherulites as for the IM_PLA samples.

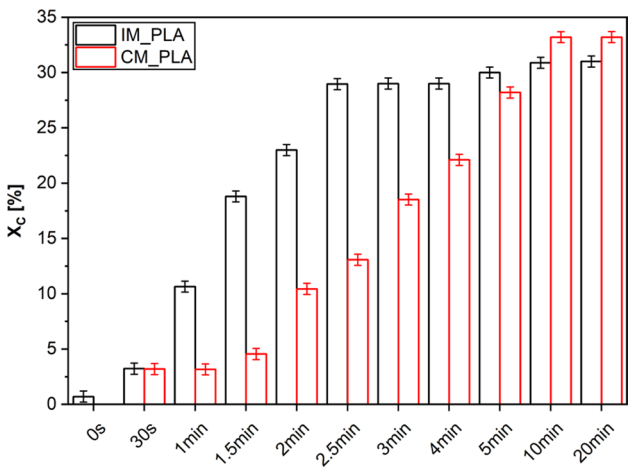

Figure 4 Crystalline contents [%] obtained by DSC for both the IM_PLA and CM_PLA samples.

Overall, PLA crystallization is characterized by two stages. During the first stage, the system will be characterized by a small number of crystallite structures without a complete spherulitic development. Afterward, during the second stage, crystal growth is merely diffusion-controlled by the polymeric chains reptation motions [33, 34]. Thus, by again considering the longer mould holding time for CM_PLA samples, this factor may have favored the promotion of stronger interactions between the polymer chains, thus enhancing their mutual arrangements into ordered domains.

Tensile characterization of IM_PLA and CM_PLA samples

Tensile results of the performed mechanical tests on the IM_PLA and CM_PLA samples are reported in Fig. 5. Mechanical data considerably differ due to the crystallinity increases. Higher crystalline content results in more regular structures, supporting the well-known fact that chain regularity leads to proportionally higher elastic moduli [35] and lower stress and elongation at break values [31].

The stress and elongation at break values are higher for the compression moulded samples. Conversely, for the injection moulded specimens, these values are lowered. This evidence can be correlated to both the higher crystalline content and to the worsening of the granular consolidation during the processing [31]. Moreover, the presence of stress concentration sites because of the presence of “face-core [1]” and/or “micro-weld lines [36]” defects, characteristic of injection moulded samples, can also be accountable for lower stress and elongations at break values.

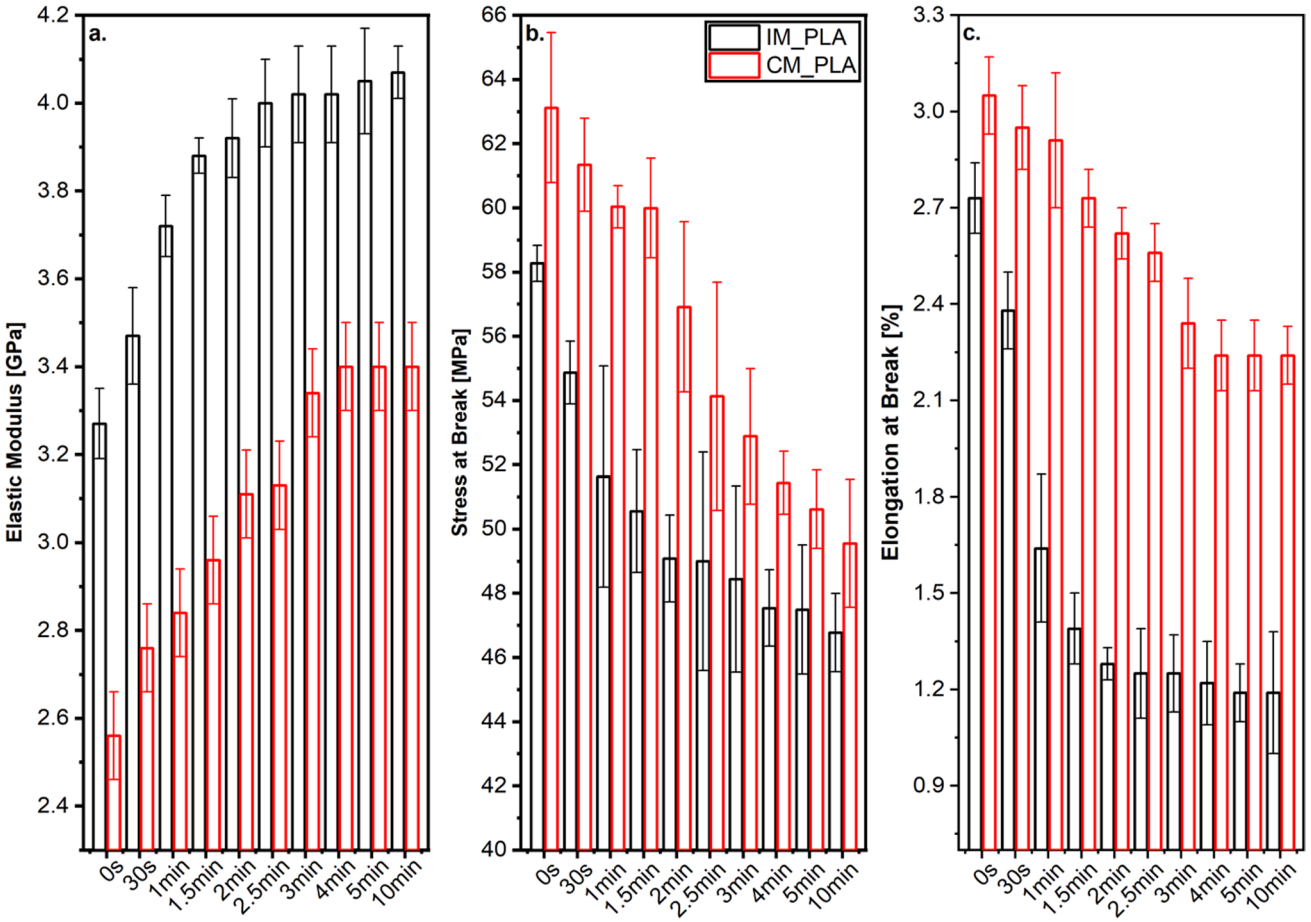

Figure 5 **a** Elastic modulus, **b** stress at break, **c** elongation at break trends for both the IM_PLA and CM_PLA samples.

The increment of Young's modulus values for the injection moulded samples can be both attributed to higher crystalline contents and to the occurrence of morphologically elongated spherulites which originate in the front-face zones of the IM_PLA specimens [26], acting as reinforcing agents. In addition, as it will be discussed in the section of XRD analysis, the crystal form of the IM_PLA and CM_PLA samples is different. The more compact α-form (IM_PLA) leads to stronger amorphous/crystalline phase couplings, hindering the relaxation of amorphous segments and thus resulting in higher stiffness [37]. In contrast, the less compact α'-form (CM_PLA) hinders the relaxation of amorphous segments to a lesser extent by promoting stress and elongations at break, as identifiable in Fig. 5.

FTIR analysis of IM_PLA and CM_PLA samples

The IR absorption around 1750 cm^{-1} is sensitive to polyesters chains conformation [38] and to their intra and inter-molecular interactions between the polymer chains [39]. Figure 6a, b, d, e depict the IR spectra (1780–1720 cm^{-1}) and the corresponding second derivates of the related C=O stretching band for both the IM_PLA and CM_PLA samples. A blue-shift toward higher wavenumbers and a gradual change in the peak shape as the crystalline content increase is detectable (Fig. 6a, d), varying from being more symmetrical toward lower wavenumbers to be more asymmetrical toward higher wavenumbers. This behavior, more

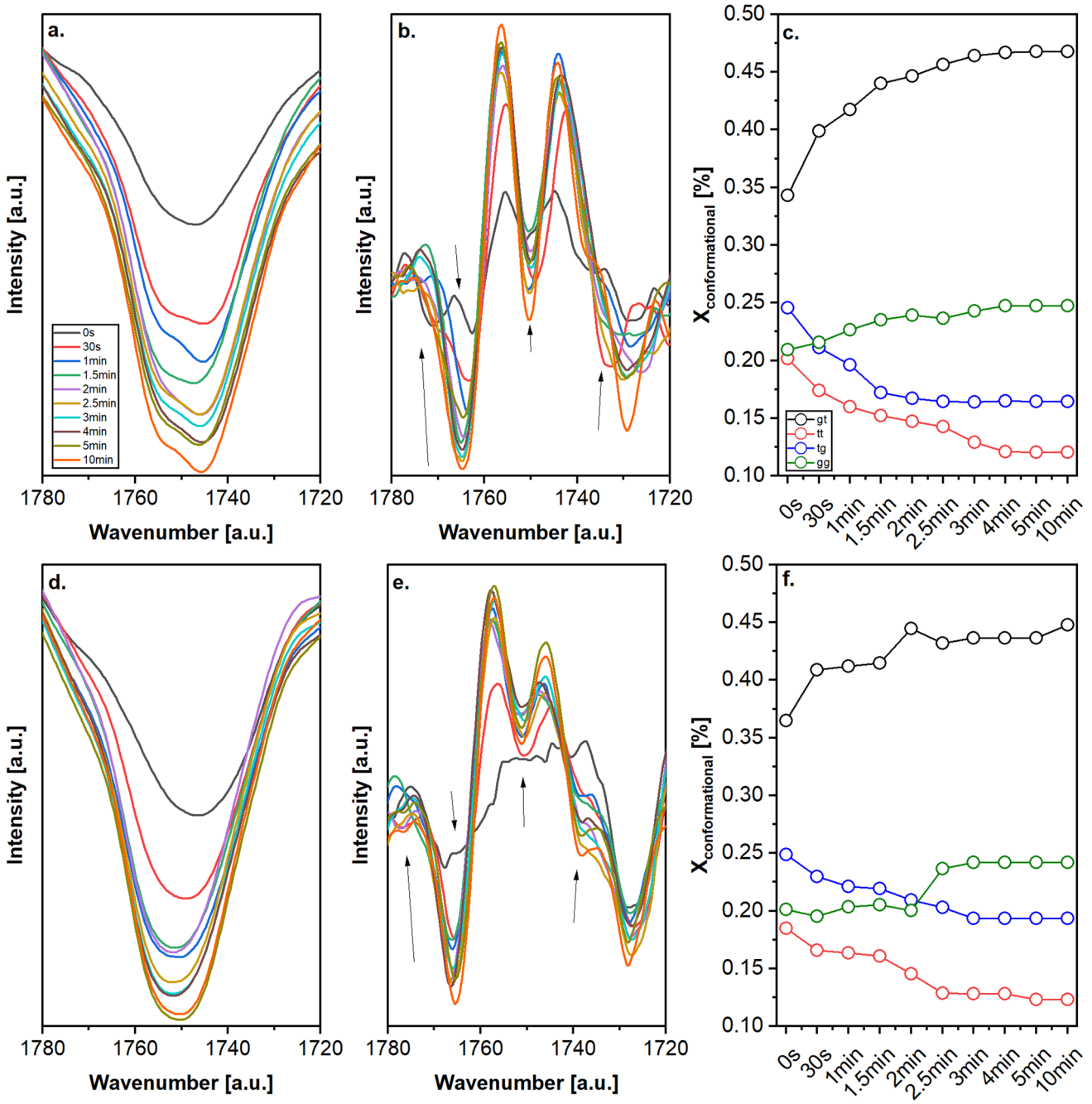

Figure 6 FTIR spectra (1780 to 1720 cm^{-1}) IR spectra and the corresponding second derivates of the (C=O) stretching band (1780–1720 cm^{-1}) for both the **a**, **b**. IM_PLA and **d**, **e**. CM_PLA samples. **c**, **f** Conformational trends for injection moulded and compression moulded PLA.

pronounced in the case of IM_PLA specimens, is generally related to the PLA chains conformations in their own arranging into ordered crystalline domains [40, 41].

By double differentiating the 1750 cm^{-1} peak (Fig. 6b, e), together with the distinct band located at 1750(1) cm^{-1}, three new bands appear at 1739, 1764(5) and 1771(6) cm^{-1}, respectively (black arrows). Meaurio et al. [40] proposed that the multiplicity associated with the υ(C=O) band is ascribable to the intramolecular coupling and/or to the splitting of the correlation field caused by interchain contact. In addition, these

bands can be directly related to *gg*, *tg*, *gt*, and *tt* chain conformers content of PLA where *tt*, *tg*, and *gg* conformers generally related to its amorphous phase while the *gt* ones to the crystalline one.

Figure 6c, f display the derivates extracted trends for the chain conformer content for the IM_PLA and CM_PLA samples. For both the injection and compression moulded samples, the contents corresponding to the derivate located at 1764(5) cm^{-1} and 1739 cm^{-1} show a decrease with the increment of the mould holding time. Conversely, for the 1750(1) cm^{-1} band, a steadily increase is detectable. The trend associated with the *gg*-conformer content (1770 cm^{-1}), rises but with a lesser extent when compared with the *gt*-related trend. It is not possible to univocally assign its contribution to the amorphous or to crystalline phase of PLA, conceivably because it outcomes of both phases contributions [42]. It is also interesting to note that the crystalline development kinetics, investigated by thermal analysis, is also correlated with conformational changes of the PLA chains. Indeed, significant variations in chain conformer contents precisely occur in the 1–1.5-time interval for IM_PLA samples and in the 2.5/3 min time interval for CM_PLA ones, thus around the half-time of crystallization estimated from the by the Avrami approach.

XRD analysis

The XRD patterns of the IM_PLA_10min and CM_PLA_10min samples are shown in Fig. 7. For the injection moulded samples, the XRD pattern exhibits the typical XRD profile of the α-form, identified by the position of the most intense (110/200) and (203/113) peaks at the 2θ scattering angles of 16.6° and 19.0°, and by the (011) and (211) peaks at 14.7° and 22.3°, as well as for several other less intense reflections at higher angles. On the other hand, PLA samples prepared by compression moulding uniquely displays the characteristic patterns of the α'-form, recognizable by the position of the most intense (110/200) and (203/113) peaks, respectively, shifted at 16.5° and 18.8°, with respect to the α-form ones. In addition, the presence of the peculiar α'-form (206/116) peak at 24.5° is well evident.

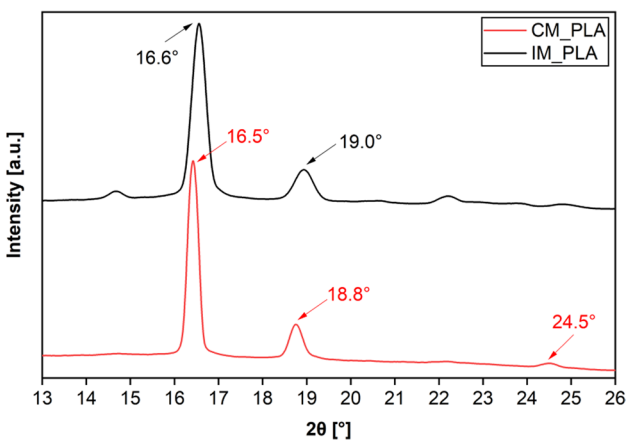

Figure 7 XRD pattern of the IM_PLA and CM_PLA samples isothermally crystallized for a mould holding time of 10 min.

According to the XRD pattern presented in Fig. 7, the average crystallographic parameters of the PLA orthorhombic cell were calculated by combining the Bragg's law with Eq. 7 [43]. The geometrical characteristics of the (011), (200) and the (203) planes for the IM_PLA, and the (110), (203) and the (203) planes for the CM_PLA ones were used to estimate the unit cell parameters, as identifiable in Table 2.

$$\left(d_{hkl}\right)^{-2} = (h/a)^2 + (k/b)^2 + (l/c)^2 \quad (7)$$

The mean crystallographic parameters of the both IM_PLA and CM_PLA samples are in a good agreement to those reported in literature for the PLA orthorhombic unit cell [44]. The slight differences between the IM_PLA samples and the CM_PLA ones are explained by changes in chain conformation and in the relative packing mode occurring during crystallization. Indeed, it is well-known that the α'-crystals are more disordered than the α-ones, resulting in a less compact unit cell. This confirms the greater cell volume value estimated for CM_PLA specimens. Remarkably, the a- and b-axis lengths of the CM_PLA samples are like those of the IM_PLA ones, implying that the distances between neighboring chains are almost identical. On the contrary, there is a difference related to the length of the c-axis. As reported by Wasanasuk

Table 2 Unit Cell Parameters of IM_PLA and CM_PLA samples estimated by XRD analysis

Sample	*a* (Å)	*b* (Å)	*c* (Å)	Cell Volume ($Å^3$)
IM_PLA	10.70 ± 0.02	6.07 ± 0.01	28.95 ± 0.04	1880 ± 9
CM_PLA	10.72 ± 0.01	6.12 ± 0.02	29.11 ± 0.03	1910 ± 11

et al. [45] and Kawai et al. [46] the conformation of the α-form with the up and down helices alternately packed could deviate into the α'-one even due to a single up/down helix. This deviation generally involves c-axial-translational motion [47], here detectable as diverse values of c-axis lengths for injection and compression moulded samples.

The XRD patterns at T_{room} of both injection and compression moulded PLA samples at different mould holding time are shown in Fig. 8. The crystalline contents, calculated from the entire XRD profiles, are comparable to those estimated by means of the thermal analysis (Fig. 4). For IM_PLA samples, greater crystalline contents are achieved more quickly without a progressive trend, showing net differences in the 1–1.5 min range of mould holding time. By contrast, for the CM_PLA samples, higher final crystalline content (at 5–10 min of the mould holding time) are reached, with respect to what detected for IM_PLA sample, with an incremental gradual trend.

It is also interesting to notice the presence of the (110/200) peak for the amorphous (0 s) IM_PLA sample (Fig. 8a), absent for the corresponding CM_PLA one. This evidence confirms that, even in absence of any annealing, the presence a chain alignment is induced by the injection moulding [48] which promotes the polymeric chains arrangements into ordered domains. These, acting as nucleation sites for crystallization, speeds up the kinetics [49] of the IM_PLA samples which result faster when compared to the one for CM_PLA samples.

TEM analysis of the IM_PLA and CM_PLA crystallization kinetics

As described in the previous study [26], the spherulitic structures of poly (lactic acid), isothermally crystallized at 110 °C, is divided into two perpendicularly oriented regions: One that looks like flat pebble-like lamellae (FPL) and the other, consisting of fibrous lamellae dendritic (FDL), with branch-like growth (Fig. 9u). FDL regions occupy larger areas, extending to more peripheral areas of the spherulite, bending and branching outward from the nucleation center. In contrast, FPL regions show smooth, packed pebble-like structures of different shapes. They originate

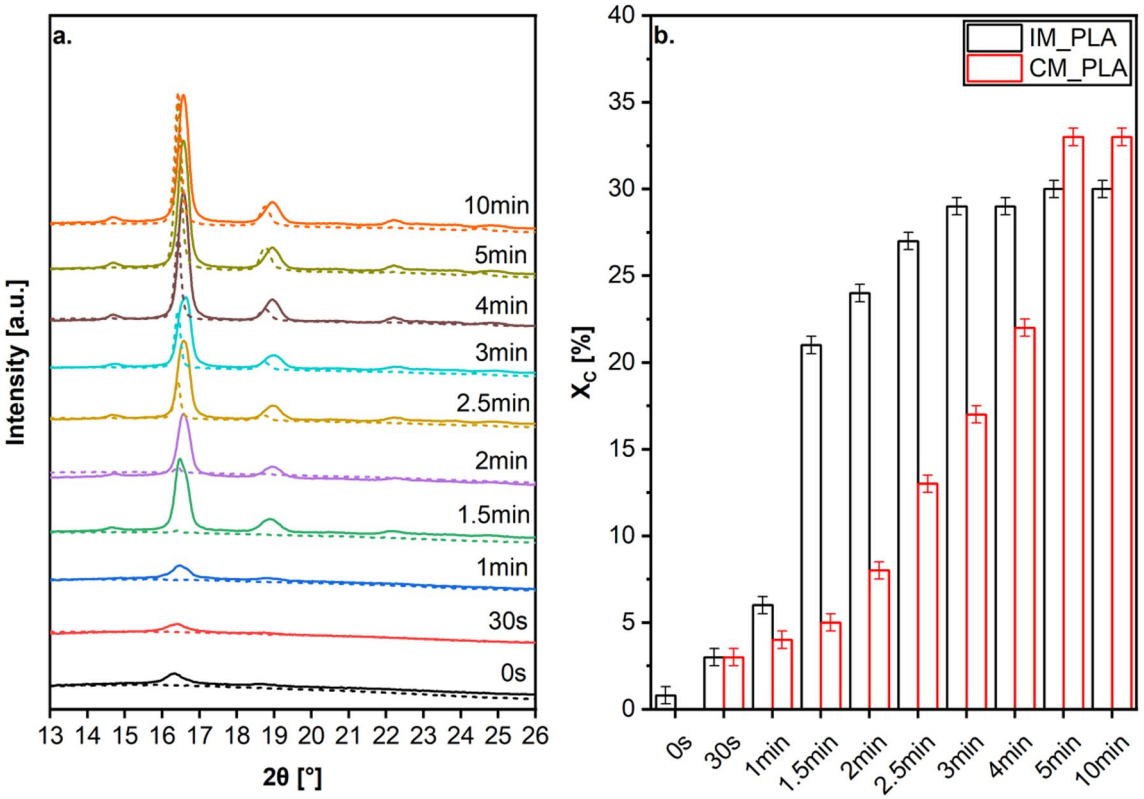

Figure 8 **a** XRD patterns and **b** crystalline contents [%] (extracted from the XRD pattern). In **a** solid lines represent the XRD spectra of IM_PLA samples instead the dashed lines represent the XRD spectra of CM_PLA one at different mould holding times.

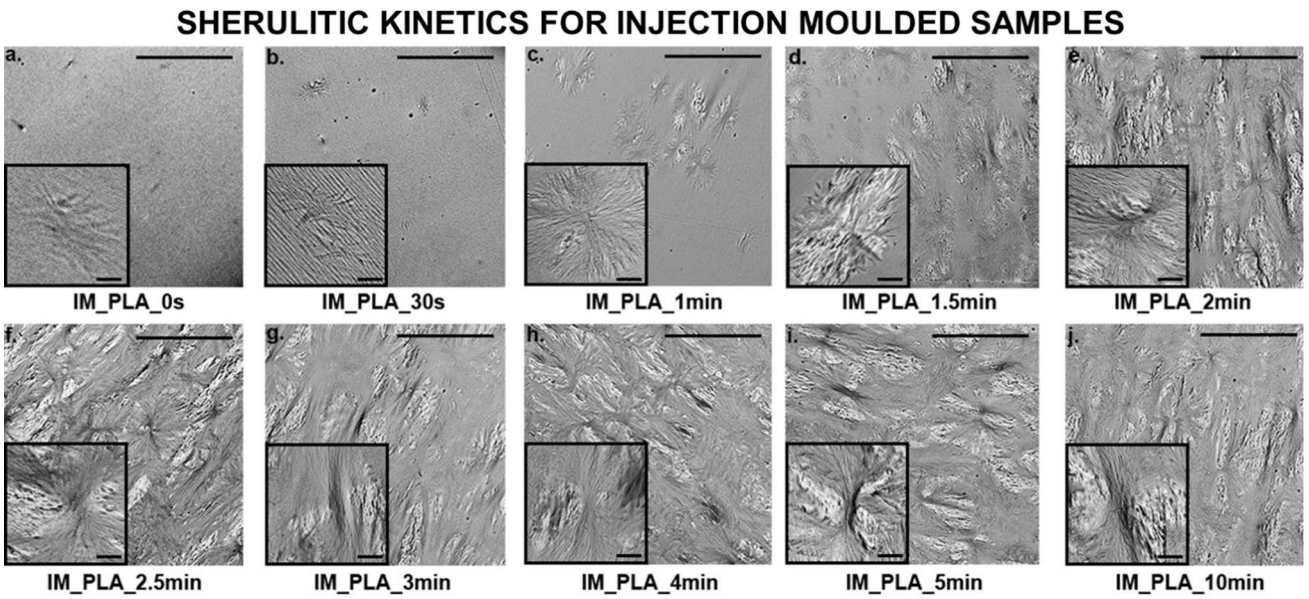
SHERULITIC KINETICS FOR INJECTION MOULDED SAMPLES
a.
b.
c.
d.
e.
IM_PLA_0s
IM_PLA_30s
IM_PLA_1min
IM_PLA_1.5min
IM_PLA_2min
f.
g.
h.
i.
j.
IM_PLA_2.5min
IM_PLA_3min
IM_PLA_4min
IM_PLA_5min
IM_PLA_10min

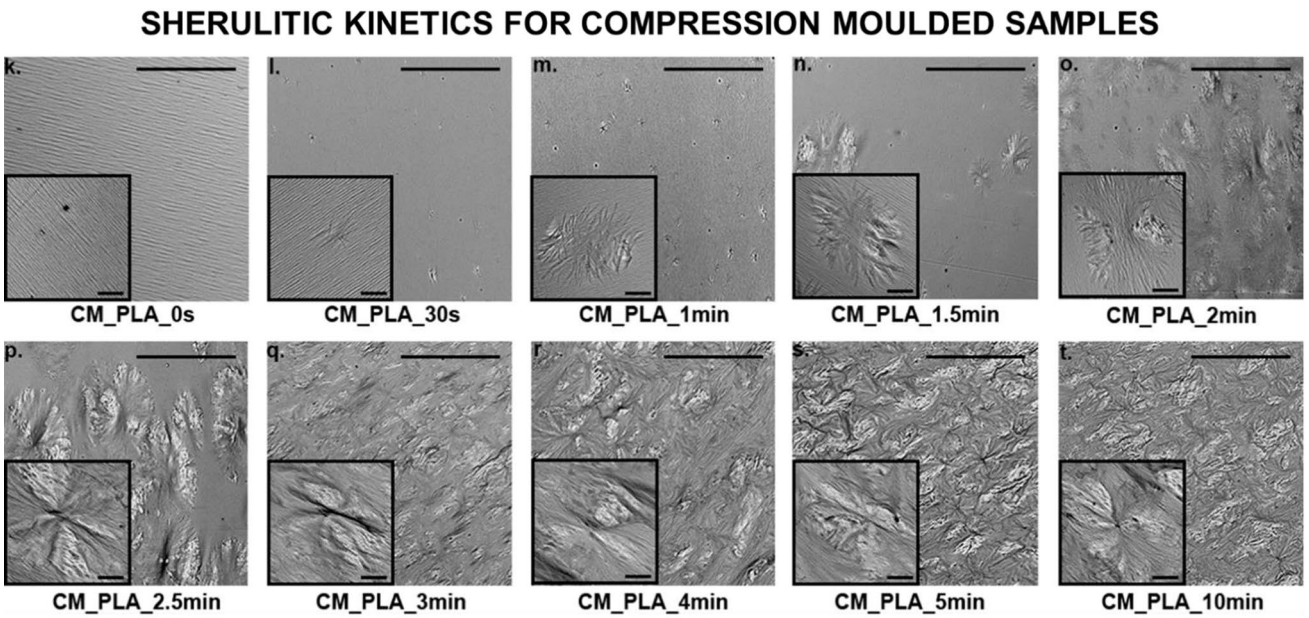
SHERULITIC KINETICS FOR COMPRESSION MOULDED SAMPLES
k.
l.
m.
n.
o.
CM_PLA_0s
CM_PLA_30s
CM_PLA_1min
CM_PLA_1.5min
CM_PLA_2min
p.
q.
r.
s.
t.
CM_PLA_2.5min
CM_PLA_3min
CM_PLA_4min
CM_PLA_5min
CM_PLA_10min

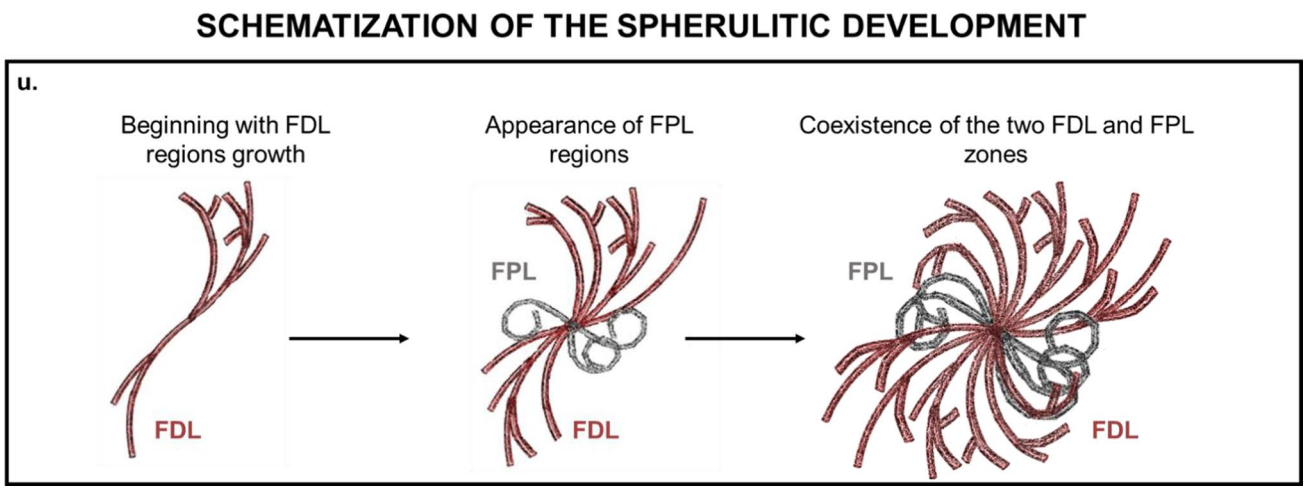
SCHEMATIZATION OF THE SPHERULITIC DEVELOPMENT
u.
Beginning with FDL regions growth
Appearance of FPL regions
Coexistence of the two FDL and FPL zones
FDL
FPL
FDL
FPL
FDL

◂**Figure 9** **a**–**j** Development of a polymer spherulite at different mould residence time for IM_PLA: **a** 0 s, **b** 30 s, **c** 1 min, **d** 1.5 min, **e** 2 min, **f** 2.5 min, **g** 3 min, **h** 4 min, **i** 5 min, **j** 10 min. **k**–**t** Development of polymer spherulite at different mould residence time for CM_PLA: **k** 0 s, **l** 30 s, **m** 1 min, **n** 1.5 min, **o** 2 min, **p** 2.5 min, **q** 3 min, **r** 4 min, **s** 5 min, **t** 10 min. Scale bars are 10 μm for lower magnification micrographs. Inset scale bars are 1 μm. **u** Graphical schematization of the semi-crystalline development.

from the same nucleation center, developing into an "eye-like" geometry zone, which boundaries are determined by the surrounding FDL-sheafs.

The kinetics of the spherulitic development for the IM_PLA and CM_PLA samples is shown in Fig. 9. For both the moulding procedures, the spherulitic growth starts with the formation of dendritic fibrous lamellar bundles (FDL), which begin to twist as the mould holding time increases, forming flat pebble lamellar (FPL) or "eye-like" regions of a gradually greater extent. FPL regions require longer time to be well-formed for CM_PLA samples (Fig. 9n, o) compared to IM_PLA ones (Fig. 9b, c). This is in accordance with a longer crystallization kinetics, as detected by thermal and XRD analyses.

It is also interesting to note that in Fig. 9a, the presence of some spherulitic-like structures, even in absence of any annealing, can be identified. This sample should be entirely amorphous but, as pointed out in the previous sections, injection moulding procedure induces a sort of chain alignment that promotes the polymeric chains arrangements into ordered domains, acting as nucleation sites for crystallization. This observation is, in fact, evidenced by the presence of the XRD peak (110/200) at 16.6° for the IM_PLA with the mould holding time of 0 s.

The transition from a predominantly dendritic morphology (FDL) to the appearance of pebble-like zones (FPL) correlates with changes in mechanical and thermal features of the both the IM_PLA and CM_PLA samples. For instance, increases in the crystalline content values and marked changes in mechanical properties (Fig. 5), as well as in FTIR conformers analysis (Fig. 6e, f), occur when lamellar twisting begins to develop: at 30 s/1 min/1.5 min mould holding times for IM_PLA samples (Fig. 9b–d) and at 1.5/2 min/2.5 min mould holding times for CM_PLA ones (Fig. 9o–q). This highlights how ultrastructural changes are directly related with variation of the macroscopic behavior of the biopolymer.

Ordered lamellar arrangements strongly improve the mechanical behavior [50], because of better load transfer among them. Moreover, a regular lamellar packing can act as a real "physical barrier" that can hinder eventual crack propagations [48], thus resulting in an enhanced mechanical strength. Here, for both IM_PLA and CM_PLA samples, this already occurs at low mould holding times (Fig. 5b, c), confirming that this evidence is not only related to the crystalline content but also to the lamellar arrangement, which at low mould holding times is purely FDL.

The different lamellar arrangement which affect the chains packing due to interactions such as hydrogen bonding or van der Waals forces between them [26], can also influence the position and intensity of specific bands in the FTIR spectrum [51]. For instance, in regions where chains are tightly packed (as in FPL regions due to the lamellar twisting), mobility may be limited, directly affecting the dynamics of vibrational modes observed in IR spectra [52].

Finally, the presence of more ordered and/or oriented lamellae (i.e., FDL) also contributes to the overall thermal stability of the polymer [53]. The more ordered the crystal structure, the higher the temperature that the polymer can withstand before undergoing significant degradation [15]. In addition, polymers with highly oriented lamellar arrangements tend to have lower coefficients of thermal expansion [54], rendering them more dimensionally stable over a wider range of temperatures [22].

TEM characterization of the IM_PLA and CM_PLA spherulitic crystalline morphology

A detailed TEM morphometrical characterization of PLA spherulitic structural evolution was also performed. By sampling an area of 2000 μm^2 over three TEM images for each sample, it was possible to estimate and compare the number of spherulites and their area, as shown in Fig. 10a, b. Spherulitic structures at the edge of the area were excluded from the sampling, as it was not possible to estimate their entire dimensions. According to the previous study [26], to properly compare the spherulites sizes, PLA thin sections were cut along the direction of the polymer melt flow during the processing (Fig. 2), "front face" for IM and "flat face" for CM). For IM_PLA samples.

The detected number of spherulites/2000 μm^2 area is lower than that for CM_PLA one; while, the spherulites area values are higher than what noticeable for

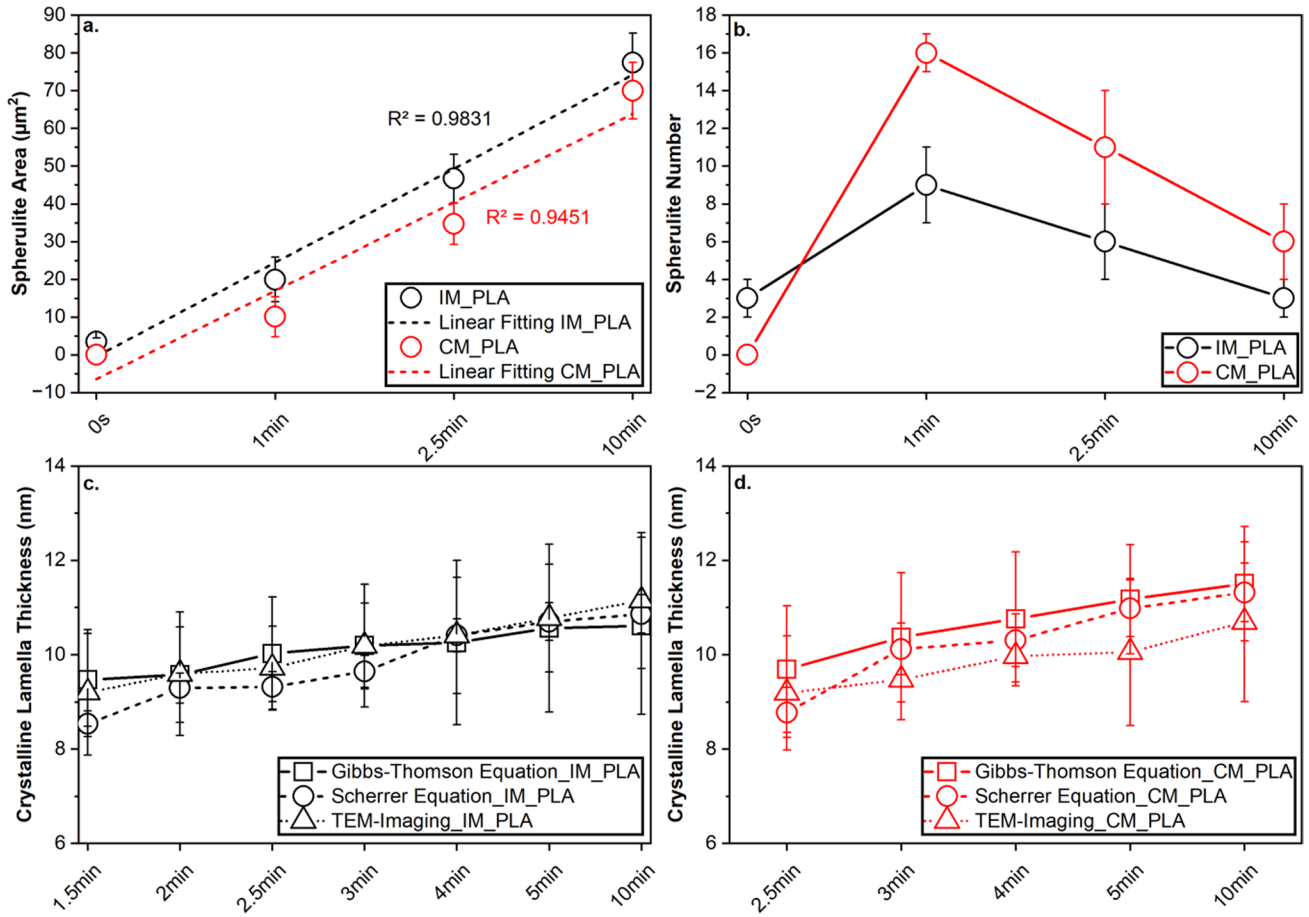

Figure 10 **a** Spherulites area and **b** number measured on TEM micrographs of IM_PLA and CM_PLA sections, parallel cut to the polymer flow direction. Lamellar thickness estimated by Gibbs–Thomson equation, TEM imaging and Scherrer equation for **c** IM_PLA and **d** CM_PLA samples.

compression moulded specimens (Fig. 10a, b). Higher spherulitic area for IM_PLA samples can be accounted by kinetic considerations. In fact, for the IM_PLA samples with the mould holding time of 0 s, the presence of small crystalline content (nuclei) is detectable, as also identified by XRD analysis and TEM imaging analysis (presence of crystalline nuclei). So, in this "moulding case," the crystalline nucleation can be considered as immediate, also with the absence of any annealing step during which the spherulitic growth generally occur. By contrast, for CM_PLA samples, nucleation is not immediate, and the annealing process includes both nucleation and growth, which proceeds with a certain delay when compared with the one during injection moulding, thus resulting in lower spherulitic area values.

This last evidence also confirms what estimated by means of the Avrami approach. The Avrami exponent n depends on dimensionality of growth and on whether nucleation is instantaneous or sporadic. The n value can be expressed as $n = n_N + n_G$, where n_N and n_G embed the nucleation and the growth components, respectively. If the nucleation is instantaneous, then $n_N = 0$, while for continuous nucleation $n_N = 1$. For IM_PLA, nucleation is instantaneous ($n_N = 0$). Hence, a final n value equal to 3.1 was detected, as the growth is homogeneous ($n_G = 3$) in the three dimensions characteristic of the injection specimen geometry. For CM_PLA, n should be equal to 4 because nucleation is not instantaneous but continuous. However, as pointed out in "*Preliminary Isothermal Kinetical Measurements*" section, the growth is strongly restricted by the 2D geometry of the compression moulded specimen ($n_G = 2$). Hence, n values equal 2.6.

The contribution of the better granular consolidation [31] and of the longer mould holding time,

characteristic of compression moulding processing, are also parameters that favor the crystalline phase development, as detectable by an higher number of spherulite for compression moulded with respect to injection moulded one (Fig. 10b) [50]. Moreover, the moulding pressure used during compression moulding is higher with respect to the one used during injection moulding due to the load and compressive actions applied during the pressing stage (Fig. 1). Higher pressures influence the characteristic relaxation times of polymer systems [55, 56]: polymer chains require longer time to structurally arrange themselves into crystalline domains (i.e., longer crystallization kinetics) giving rise to lower spherulites areas as detected for the CM_PLA samples (Fig. 10a).

Finally, it is important to also consider the influence of the moulded sample thickness, as it can directly affect the polymeric crystallinity. According to Kahouli's analysis [57] and Evans' theory of growth and nucleation [58], as the moulded sample thickness increases, the crystalline development is favored due to the minimization of surface energy. This theoretical consideration coincides with the experimental evidence highlighted here: IM_PLA (thicker) specimens exhibit structures whose area values are greater than those found for CM_PLA (thinner) specimens.

Comparison between TEM imaging and theoretical Gibbs–Thomson and Scherrer equation Lamellar thickness for IM_PLA and CM_PLA samples

According to the study of Schick et al. [59] and Furushima et al. [60], by exploiting the Gibbs–Thomson (G–T) equation [61, 62] (Eq. 8), it is possible to quantitatively assess the lamellar thickness of the polymeric systems:

$$T_m = T_{m,0} \cdot \left(1 - \frac{2\sigma_e}{l_c \Delta h_{m,0}}\right) \quad (8)$$

where σ_e, l_c and $\Delta h_{m,0}$ represent the surface free energy of the lamellar crystal, the lamellar thickness, and the melting enthalpy per unit of volume, respectively. $T_{m,0}$, $\Delta h_{m,0}$ and σ_e are constants well reported in literature for PLA [63] as 166.8 °C, 141 J/g and 0.0372 J m^{-2}, respectively.

The lamellar thickness values obtained from the G-T equation were compared with those from the TEM imaging and from the application of the Scherrer equation (Eq. 1), by sampling 20 FDL-like lamellae of five spherulites within the same injection or compression moulded specimens (Fig. 10c, d). It can be observed that for both IM_PLA and CM_PLA samples there are slight differences between the values obtained by applying the G–T equation and by the evaluation performed from the thermal measurements. Remarkable, TEM imaging gives a direct view of the lamellar size showing, as for the other quantifications methodologies carried out (Scherrer and G–T equations), incremental trends at increases in mould holding time/crystalline contents. This evidence is explained by the well-known phenomenon of "lamellar thickening," where the crystalline fraction in the lamellar stack thickens once the crystalline content increases [64, 65].

Conclusions

Moulding processing of poly (lactic acid) (PLA) is crucial for its end-products features. Indeed, a precise control over diverse moulding parameters can ensure optimal mechanical behavior, and dimensional stability. By contrast, an inadequate processing can lead to defects like warping, brittleness, or incomplete filling, compromising performance and durability.

This work investigates the impact of two different processes, injection (IM) and compression moulding (CM), attempting to determine their influence on the macroscopical behavior of differently moulded PLA specimens. So, by means of thermal, mechanical and microscopy analysis, the role of diverse mould holding times/crystalline content (at the crystallization temperature T = 110 °C) in influencing the PLA semi-crystalline development will be extensively investigated.

The thermal and mechanical behavior, in both injection and compression moulding, show regular trends in elastic modulus, stress and elongation at break values as the mould holding time/crystalline content is increased. Moreover, the analysis of crystalline phase kinetics, together with microscopic evaluations performed by XRD analysis and TEM imaging, allow not only to "characterize" the crystallization development in detail but also to link changes in macroscopic behavior to variations in the morphology of spherulitic structures for both the two types of employed moulding techniques. For instance, the development of pebble-like lamellar (FPL) structures following dendritic lamellar (FDL) ones has been found to occur in correspondence to differences in mechanical and thermal characteristics trends.

As evidenced using Avrami approach, XRD measurements and TEM imaging, injection moulding is more likely to promote the crystalline nucleation stage even in absence of any annealing stage, due to a sort of chain alignment into ordered domains, induced by the polymer flow during the melt injection. Contribution of the mould sample thickness is an additional parameter that also promote a faster crystallization for IM when compared with the CM. By contrast, higher pressure and a longer mould holding time before annealing facilitates the crystalline growth for the compression moulded samples. Finally, a direct sampling via TEM imaging together with theoretical models (i.e., Scherrer and Gibbs–Thomson equations) of the lamellar thicknesses, allows to identify the phenomenon of "lamellar thickening" and to correlated it with increasing in the crystalline content of the samples.

The study lays the foundation for a better understanding of the impact of two of the most utilized moulding methodologies of PLA on the macro- and micro-behaviors of its end-product, so that they can be predicted and, therefore, optimized with a view to improving their final performances.

Author contributions

Molinari Giovanna contributed to conceptualization, data curation, investigation, methodology, writing—original draft, and writing—review and editing. Laura Aliotta contributed to conceptualization, data curation, investigation, methodology, validation, and writing—review and editing. Parlanti Paola contributed to conceptualization, data curation, investigation, methodology, validation, and writing—review and editing. Gemmi Mauro contributed to conceptualization, funding acquisition, supervision, writing—review and editing. Lazzeri Andrea contributed to conceptualization, funding acquisition, supervision, writing—review and editing.

Data Availability

Data will be made available on request.

Declaration

Conflict of interest The authors declare that they have no known competing financial interests or personal relationships that could have appeared to influence the work reported in this paper.

References

[1] Gim J, Turng L-SS (2022) A review of current advancements in high surface quality injection molding: Measurement, influencing factors, prediction, and control. Polym Test 115:107718. https://doi.org/10.1016/j.polymertesting.2022.107718

[2] Courgneau C, Domenek S, Guinault A, Avérous L, Ducruet V (2011) Analysis of the structure-properties relationships of different multiphase systems based on plasticized poly(lactic acid). J Polym Environ 19:362–371. https://doi.org/10.1007/s10924-011-0285-5

[3] Jandas PJ, Prabakaran K, Mohanty S, Nayak SK (2019) Evaluation of biodegradability of disposable product prepared from poly (lactic acid) under accelerated conditions. Polym Degrad Stab 164:46–54. https://doi.org/10.1016/j.polymdegradstab.2019.04.004

[4] Kuei B, Aplan MP, Litofsky JH, Gomez ED (2020) New opportunities in transmission electron microscopy of polymers. Mater Sci Eng R Reports 139:100516. https://doi.org/10.1016/j.mser.2019.100516

[5] Jem KJ, Tan B (2020) The development and challenges of poly (lactic acid) and poly (glycolic acid). Adv Ind Eng Polym Res 3:60–70. https://doi.org/10.1016/j.aiepr.2020.01.002

[6] Atiwesh G, Mikhael A, Parrish CC, Banoub J, Le TAT (2021) Environmental impact of bioplastic use: A review. Heliyon 7:e07918. https://doi.org/10.1016/j.heliyon.2021.e07918

[7] The Plastic Packaging Problem, (n.d.)

[8] Mofokeng JP, Luyt AS, Tábi T, Kovács J (2012) Comparison of injection moulded, natural fibre-reinforced composites with PP and PLA as matrices. J Thermoplast Compos Mater 25:927–948. https://doi.org/10.1177/0892705711423291

[9] Quynh TM, Mai HH, Lan PN (2013) Stereocomplexation of low molecular weight poly(L-lactic acid) and high molecular weight poly(D-lactic acid), radiation crosslinking PLLA/PDLA stereocomplexes and their characterization. Radiat Phys Chem 83:105–110. https://doi.org/10.1016/j.radphyschem.2012.10.002

[10] Höglund A, Hakkarainen M, Albertsson AC (2010) Migration and hydrolysis of hydrophobic polylactide plasticizer. Biomacromol 11:277–283. https://doi.org/10.1021/bm901157h

[11] Sharma S (2021) Polylactic acid (PLA) and its composites: an eco-friendly solution for packaging. In: Athanassiou A (ed) Sustainable food packaging technology. https://doi.org/10.1002/9783527820078.ch4

[12] Tseng CH, Tsai PS (2022) The isothermal and nonisothermal crystallization kinetics and morphology of solvent-precipitated nylon 66. Polymers (Basel) 14(3):442. https://doi.org/10.3390/polym14030442

[13] Oksiuta Z, Jalbrzykowski M, Mystkowska J, Romanczuk E, Osiecki T (2020) Mechanical and thermal properties of polylactide (PLA) composites modified with Mg, Fe, and polyethylene (PE) additives. Polymers (Basel) 12:1–14. https://doi.org/10.3390/polym12122939

[14] Cai H, Dave V, Gross RA, McCarthy SP (1996) Effects of physical aging, crystallinity, and orientation on the enzymatic degradation of poly(lactic acid). J Polym Sci Part B Polym Phys 34:2701–2708. https://doi.org/10.1002/(SICI)1099-0488(19961130)34:16%3c2701::AID-POLB2%3e3.0.CO;2-S

[15] Sreekumar K, Bindhu B, Veluraja K (2021) Perspectives of polylactic acid from structure to applications. Polym Renew Resour 12(60):74. https://doi.org/10.1177/20412479211008773

[16] Talbott MF, Springer GS, Berglund LA (1987) The effects of crystallinity on the mechanical properties of PEEK polymer and graphite fiber reinforced PEEK. J Compos Mater 21:1056–1081. https://doi.org/10.1177/002199838702101104

[17] Katogi H, Takemura K (2014) The effect of crystallinity on the mechanical properties of plain woven carbon reinforced composites using polypropylene. WIT Trans Built Environ 137:301–310. https://doi.org/10.2495/HPSM140281

[18] Aliotta L, Sciara LM, Cinelli P, Canesi I, Lazzeri A (2022) Improvement of the PLA crystallinity and heat distortion temperature optimizing the content of nucleating agents and the injection molding cycle time. Polymers (Basel) 14(5):977. https://doi.org/10.3390/polym14050977

[19] Aliotta L, Cinelli P, Coltelli MB, Righetti MC, Gazzano M, Lazzeri A (2017) Effect of nucleating agents on crystallinity and properties of poly (lactic acid) (PLA). Eur Polym J 93:822–832. https://doi.org/10.1016/j.eurpolymj.2017.04.041

[20] Renouf-Glauser AC, Rose J, Farrar DF, Cameron RE (2005) The effect of crystallinity on the deformation mechanism and bulk mechanical properties of PLLA. Biomaterials 26:5771–5782. https://doi.org/10.1016/j.biomaterials.2005.03.002

[21] Guinault A, Sollogoub C, Domenek S, Grandmontagne A, Ducruet V (2010) Influence of crystallinity on gas barrier and mechanical properties of pla food packaging films. Int J Mater Form 3:603–606. https://doi.org/10.1007/s12289-010-0842-9

[22] Guinault A, Sollogoub C, Ducruet V, Domenek S (2012) Impact of crystallinity of poly(lactide) on helium and oxygen barrier properties. Eur Polym J 48:779–788. https://doi.org/10.1016/j.eurpolymj.2012.01.014

[23] Courgneau C, Domenek S, Lebossé R, Guinault A, Avérous L, Ducruet V (2012) Effect of crystallization on barrier properties of formulated polylactide. Polym Int 61:180–189. https://doi.org/10.1002/pi.3167

[24] Jia Y, Mao Z, Huang W, Zhang J (2022) Effect of temperature and crystallinity on the thermal conductivity of semi-crystalline polymers: a case study of polyethylene. Mater Chem Phys 287:126325. https://doi.org/10.1016/j.matchemphys.2022.126325

[25] Fischer EW, Sterzel HJ, Wegner G (1973) Investigation of the structure of solution grown crystals of lactide copolymers by means of chemical reactions. Kolloid-Zeitschrift Und Zeitschrift Für Polym 251:980–990. https://doi.org/10.1007/BF01498927

[26] Molinari G, Parlanti P, Aliotta L, Lazzeri A, Gemmi M (2023) TEM morphological analysis of biopolymers: the case of poly (Lactic Acid) (PLA). Mater Today Commun 38:107868. https://doi.org/10.1016/j.mtcomm.2023.107868

[27] Yu L, Davidson E, Sharma A, Andersson MR, Segalman R, Müller C (2017) Isothermal crystallization kinetics and time-temperature-transformation of the conjugated polymer: poly(3-(2′-ethyl)hexylthiophene). Chem Mater 29:5654–5662. https://doi.org/10.1021/acs.chemmater.7b01393

[28] Lu F, Yu H, Yan C, Yao J (2016) Polylactic acid nanocomposite films with spherical nanocelluloses as efficient nucleation agents: Effects on crystallization, mechanical and thermal properties. RSC Adv 6:46008–46018. https://doi.org/10.1039/c6ra02768g

[29] Lorenzo AT, Arnal ML, Albuerne J, Müller AJ (2007) DSC isothermal polymer crystallization kinetics measurements and the use of the Avrami equation to fit the data: Guidelines to avoid common problems. Polym Test 26:222–231. https://doi.org/10.1016/j.polymertesting.2006.10.005

[30] Ji F, Li J, Weng Y, Ren J (2020) Synthesis of PLA-based thermoplastic elastomer and study on preparation and properties of PLA-based shape memory polymers. Mater Res Express 7:015315. https://doi.org/10.1088/2053-1591/ab61a8

[31] Xie HLM, Chen J (2010) Morphology and mechanical properties of injection-molded ultrahigh molecular weight polyethylene/polypropylene blends and comparison with compression molding. J Appl Polym Sci 116:2658–2667. https://doi.org/10.1002/app

[32] Simmons DS (2016) An emerging unified view of dynamic interphases in polymers. Macromol Chem Phys 217:137–148. https://doi.org/10.1002/macp.201500284

[33] Chen Z, Hay JN, Jenkins MJ (2016) The effect of secondary crystallization on crystallization kinetics—polyethylene terephthalate revisited. Eur Polym J 81:216–223. https://doi.org/10.1016/j.eurpolymj.2016.05.028

[34] Seo J, Zhang X, Schaake RP, Rhoades AM, Colby RH (2021) Dual Nakamura model for primary and secondary crystallization applied to nonisothermal crystallization of poly(ether ether ketone). Polym Eng Sci 61:2416–2426. https://doi.org/10.1002/pen.25767

[35] Polińska M, Rozanski A, Galeski A, Bojda J (2021) The modulus of the amorphous phase of semicrystalline polymers. Macromolecules 54:9113–9123. https://doi.org/10.1021/acs.macromol.1c01576

[36] Liparoti S, De Piano G, Salomone R, Pantani R (2023) Analysis of weld lines in micro-injection molding. Materials (Basel) 16(17):6053. https://doi.org/10.3390/ma16176053

[37] Zhang J, Tashiro K, Tsuji H, Domb AJ (2008) Disorder-to-order phase transition and multiple melting behavior of poly(L-lactide) investigated by simultaneous measurements of WAXD and DSC. Macromolecules 41:1352–1357. https://doi.org/10.1021/ma0706071

[38] Lee HW, Insyani R, Prasetyo D, Prajitno H, Sitompul J (2015) Molecular weight and structural properties of biodegradable PLA synthesized with different catalysts by direct melt polycondensation. J Eng Technol Sci 47:364–373. https://doi.org/10.5614/j.eng.technol.sci.2015.47.4.2

[39] Partini M, Pantani R (2007) Determination of crystallinity of an aliphatic polyester by FTIR spectroscopy. Polym Bull 59:403–412. https://doi.org/10.1007/s00289-007-0782-9

[40] Meaurio E, López-Rodríguez N, Sarasua JR (2006) Infrared spectrum of poly(L-lactide): application to crystallinity studies. Macromolecules 39:9291–9301. https://doi.org/10.1021/ma061890r

[41] Zhu Z, Bian Y, Zhang X, Zeng R, Yang B (2022) Study of crystallinity and conformation of poly(lactic acid) by terahertz spectroscopy. Anal Chem 94:11104–11111. https://doi.org/10.1021/acs.analchem.2c02652

[42] Yang CF, Huang YF, Ruan J, Su AC (2012) Extensive development of precursory helical pairs prior to formation of stereocomplex crystals in racemic polylactide melt mixture. Macromolecules 45:872–878. https://doi.org/10.1021/ma2026995

[43] Farid T, Herrera VN, Kristiina O (2018) Investigation of crystalline structure of plasticized poly (lactic acid)/Banana nanofibers composites. IOP Conf Ser Mater Sci Eng 369:012031. https://doi.org/10.1088/1757-899X/369/1/012031

[44] Aliotta L, Gazzano M, Lazzeri A, Righetti MC (2020) Constrained amorphous interphase in poly(L-lactic acid): estimation of the tensile elastic modulus. ACS Omega 5:20890–20902. https://doi.org/10.1021/acsomega.0c02330

[45] Wasanasuk K, Tashiro K (2011) Crystal structure and disorder in Poly(L-lactic acid) δ form (α′ form) and the phase transition mechanism to the ordered α form. Polymer (Guildf) 52:6097–6109. https://doi.org/10.1016/j.polymer.2011.10.046

[46] Kawai T, Rahman N, Matsuba G, Nishida K, Kanaya T, Nakano M, Okamoto H, Kawada J, Usuki A, Honma N, Nakajima K, Matsuda M (2007) Crystallization and melting behavior of poly (L-lactic Acid). Macromolecules 40:9463–9469. https://doi.org/10.1021/ma070082c

[47] Pan P, Zhu B, Kai W, Dong T, Inoue Y (2008) Polymorphic transition in disordered poly(L-lactide) crystals induced by annealing at elevated temperatures. Macromolecules 41:4296–4304. https://doi.org/10.1021/ma800343g

[48] SadAbadi H, Ghasemi M (2007) Effects of some injection molding process parameters on fiber orientation tensor of short glass fiber polystyrene composites (SGF/PS). J Reinf Plast Compos 26:1729–1741. https://doi.org/10.1177/0731684407081352

[49] Pantani R, Coccorullo I, Speranza V, Titomanlio G (2005) Modeling of morphology evolution in the injection molding process of thermoplastic polymers. Prog Polym Sci 30:1185–1222. https://doi.org/10.1016/j.progpolymsci.2005.09.001

[50] Crist B, Schultz JM (2016) Polymer spherulites: a critical review. Prog Polym Sci 56:1–63. https://doi.org/10.1016/j.progpolymsci.2015.11.006

[51] Ahmed J, Varshney SK (2011) Polylactides-chemistry, properties and green packaging technology: a review. Int J Food Prop 14:37–58. https://doi.org/10.1080/10942910903125284

[52] Hirata J, Kurokawa N, Okano M, Hotta A, Watanabe S (2020) Evaluation of crystallinity and hydrogen bond formation in stereocomplex poly(lactic acid) films by terahertz time-domain spectroscopy. Macromolecules 53:7171–7177. https://doi.org/10.1021/acs.macromol.0c00237

[53] Saeidlou S, Huneault MA, Li H, Park CB (2012) Poly(lactic acid) crystallization. Prog Polym Sci 37:1657–1677. https://doi.org/10.1016/j.progpolymsci.2012.07.005

[54] Song F, Wang Q, Wang T (2016) The effects of crystallinity on the mechanical properties and the limiting PV (pressure×velocity) value of PTFE. Tribol Int 93:1–10. https://doi.org/10.1016/j.triboint.2015.09.017

[55] Spooner J, Wiebe H, Boon N, Deglint E, Edwards E, Yanciw B, Patton B, Thiele L, Dance P, Weinberg N (2012) Molecular dynamics calculation of molecular volumes and volumes of activation. Phys Chem Chem Phys 14:2264–2277. https://doi.org/10.1039/c2cp22949h

[56] Haudin JM, Boyer SAE (2017) Crystallization of polymers in processing conditions: an overview. Int Polym Process 32:545–554. https://doi.org/10.3139/217.3415

[57] Kahouli A (2012) Effect of film thickness on structural, morphology, dielectric and electrical properties of parylene C films. J Appl Phys 112(6):064103. https://doi.org/10.1063/1.4752022

[58] Piorkowska E, Galeski A, Haudin JM (2006) Critical assessment of overall crystallization kinetics theories and predictions. Prog Polym Sci 31:549–575. https://doi.org/10.1016/j.progpolymsci.2006.05.001

[59] Schick C, Toda A, Androsch R (2021) The narrow thickness distribution of lamellae of poly(butylene succinate) formed at low melt supercooling. Macromolecules 54:3366–3376. https://doi.org/10.1021/acs.macromol.1c00388

[60] Furushima Y, Nakada M, Murakami M, Yamane T, Toda A, Schick C (2015) Method for calculation of the lamellar thickness distribution of not-reorganized linear polyethylene using fast scanning calorimetry in heating. Macromolecules 48:8831–8837. https://doi.org/10.1021/acs.macromol.5b02278

[61] Pyda M, Bopp RC, Wunderlich B (2004) Heat capacity of poly(lactic acid). J Chem Thermodyn 36:731–742. https://doi.org/10.1016/j.jct.2004.05.003

[62] Phang IY, Pramoda KP, Liu T, He C (2004) Crystallization and melting behavior of polyester/clay nanocomposites. Polym Int 53:1282–1289. https://doi.org/10.1002/pi.1513

[63] Zhang RC, Sun D, Lu A, Zhong M, Xiong G, Wan Y (2017) Equilibrium melting temperature of polymorphic poly(L-lactide) and its supercooling dependence on growth kinetics. Polymers (Basel) 9(11):625. https://doi.org/10.3390/polym9110625

[64] Bassett DC, Patel D (1994) Isothermal lamellar thickening and the distribution of thermal stability in spherulitic isotactic poly(4-methylpentene-1). Polymer (Guildf) 35:1855–1862. https://doi.org/10.1016/0032-3861(94)90974-1

[65] Cheng SZD, Zhang A, Barley JS, Chen J, Habenschuss A, Zschack PR (1991) Isothermal thickening and thinning processes in low molecular weight poly (ethylene oxide) fractions. 1. From nonintegral-folding to integral-folding chain crystal transitions. Macromolecules 24:3937–3944. https://doi.org/10.1021/ma00013a030